Journal of the Ceramic Society of Japan 116 [1] 146-152 2008 Paper

Evaluation of color prediction models in the decoration of ceramic tiles

G. Peris-Fajarnés, P. Latorre,* B. Defez,† I. Tortajada and F. Brusola

Graphic Engineering Department, Polytechnic University of Valencia Camino de Vera s/n-8L, 46022 Valencia, Spain
***Informatic Languages and Systems Department, University Jaume I Campus del Riu Sec s/n, 12071 Castelláon de la Plana, Spain**

The manufacturing of ceramic tiles is a very complex process, where a wide range of variables has an important influence in the final product. With regard to external appearance, the most of the production defects take place in the decoration station. Nevertheless, these defects are usually detected before baking, when the product is already finished, causing an important loss of effectives. Under this perspective, a mechanism able to detect the printing defects in the green parts would achieve 2 goals: on one hand, the reduction of the nonquality costs since green parts can be more easily recycled; and on the other hand, it would point out the real root cause of the failure by indicating, for instance, which ink is causing the problem. Color Prediction Models (CPM) are mathematical approaches which relate the microscopic distribution of the printed dots of a halftone image with the resulting macroscopic color. Its usage is extended in the field of the Graphic Arts, especially for calibration and fine image reproduction. However, they are barely known in the ceramic tile industry, a sector that keeps many similarities with the Graphic Arts one in terms of decorating. In this paper, we analyzed the prediction quality of 4 successful CPM (Murray–Davies, Yule–Nielsen, Neugebauer and Neugebauer Modified Yule–Nielsen) on 1 and 2 inks halftones printed on ceramic substrates, setting a comparison between them by means of linear and non-linear optimization techniques. Moreover, we proposed a value for the enigmatic "n" parameter on ceramic surfaces, which is said to model the optical dot gain phenomenon.

Key-words: Color prediction models, Ceramic tiles manufacturing, Ceramic inkjet printing, Optical dot gain

[Received September 30, 2007; Accepted November 15, 2007]

1. Introduction

The manufacturing of ceramic tiles is a very complex process, where a wide range of variables, from machine parameters to environmental factors, has an important influence in the final product.[1] With regard to the external appearance, the most of the production defects take place in the decoration station, due to inaccuracies in the printing system.[2] Nevertheless, these defects are usually detected in the quality control before baking (classification) when the product is already finished,[3),4] causing an important loss of effectives due to 2 facts: on one hand, fired parts are more difficult to recycle since their materials have already sintered; on the other hand, a final part is not profitable, meaning the total uselessness of the previous process (materials, work, energy, time...money).[5]

In this context, it would be desirable the development of a mechanism able to detect the decoration defects just after printing and of course before firing. This would achieve a reduction of the costs caused by the recycling of the faulty finished parts and moreover, would be able to establish the real cause of the defect, for instance, a defective ink distribution.[6] With this information, the printing system could be intime adjusted, avoiding a chain of defective parts. It could even be the start of self-regulated printing station, which will be highly effective and reliable.

A possible tool for the correlation between the detection of printing failures and the establishment of the root cause of the same consists in the application of Color Prediction Models (CPM). Halftone is the reprographic technique used to transfer images on ceramic surfaces. This technique is based on the simulation of continuous tone imagery through the use of color dots, varying either their size or distribution[7] and it is massively used in those sectors where color reproduction is an important manufacturing phase, such as in the Graphic Arts and in the ceramic tile industries.[8),9] CPM could relate the printing dot distribution of the halftone patterns at the microscopic level with the color variation of these patterns macroscopically. Therefore, the evaluation of a printed surface with a CPM could first decide if the result is adequate and secondly, indicate the most feasible cause for discrepancy.

In this paper, we analyzed the prediction quality of 4 successful CPM (Murray–Davies, Yule–Nielsen, Neugebauer and Neugebauer Modified Yule–Nielsen) on 1 and 2 inks halftones printed on ceramic substrates, setting a comparison between them by means of linear and non-linear optimization techniques. Moreover, we proposed a value for the enigmatic "n" parameter on ceramic surfaces, which is said to model optical dot gain phenomenon.

2. Particularities of the chosen CPM

CPM are mathematical equations that calculate the reflectance curve of a color sample using several parameters. In the linear models, these parameters are the occupied area of each primary ink of the sample (a_i) and the reflectance of the same in full occupation ($R_i(\lambda)$ when $a_i = 100\%$). The non-linear models have in addition the n parameter, which is said to model the optical dot gain (apparent growth of the dot due to the dispersion of the light on a particular surface) and therefore, should be characteristic of the substrate's nature (i.e. n would be different for paper and for ceramics).

† Corresponding author: B. Defez; E-mail: bdefez@degi.upv.es

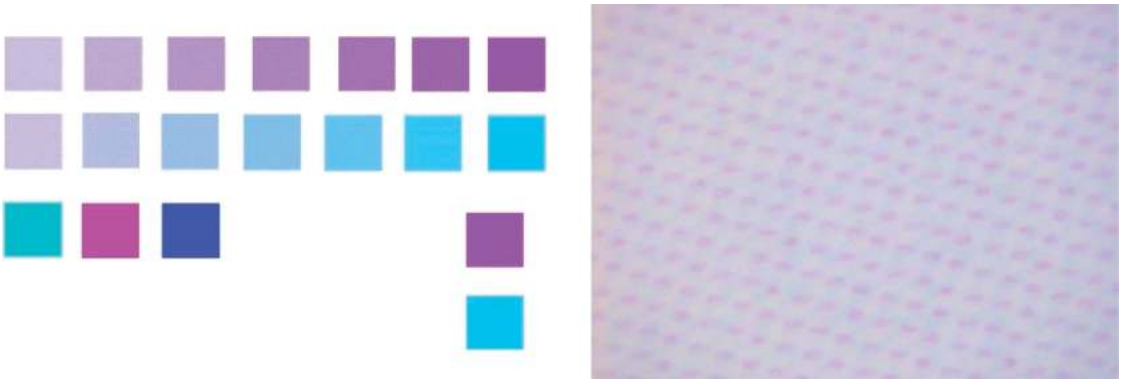

Fig. 1 Color samples for the primaries cyan and magenta.

The chosen CPM are well known in the field of the Graphic Arts[10] and have successfully served on calibration and fine image reproduction. They can be expressed as follows:

For 1 ink:

—Murray–Davies Model

$$R(\lambda) = a_1 \cdot R_1(\lambda) + (1 - a_1) \cdot R_2(\lambda)$$

—Yule–Nielsen

$$R(\lambda)^{1/n} = a_1 \cdot R_1(\lambda)^{1/n} + (1 - a_1) \cdot R_2(\lambda)^{1/n}$$

For 2 inks:

—Neugebauer:

$$R(\lambda) = \Sigma_i\, a_i \cdot R_i(\lambda)$$

—Neugebauer Modified Yule–Nielsen

$$R(\lambda)^{1/n} = \Sigma_i\, a_i \cdot R_i(\lambda)^{1/n}$$

3. Experimental approach

Now that the structure of the selected CPM has been exposed, we present the approach of our research.

First, we created a set of color samples of 1 and 2 inks halftones, and printed them on ceramic substrates. Then, the reflectance curve of each sample was physically measured (experimental curves), as much as those of the primaries in full occupation ($R_i(\lambda)$). With these data, we estimated, applying mathematical optimization techniques, the $\{a_i, n\}$ parameters. Next, we built the 4 CPM and calculated the new reflectance curves as established by the models (analytic curves). Finally, we compared the results of both experimental and analytic curves with regard to different merit figures (errors) to conclude which models are more appropriate for ceramic tiles, and which is a suitable value for n, which only depends on the nature of the surface.

In the following paragraphs we explain in detail this procedure.

4. Samples manufacturing

4.1 Creation of the digital files

For the printing of the halftone designs, we created digital files corresponding to a theoretical printing surface of 20×30 cm^2, on which we generated 3×3 cm^2 color samples of 1 and 2 inks (cyan, magenta, yellow and black or just C, M, Y and K). The resolution of the pictures was 180 dpi (dots per inch) and 60 lpi (lines per inch). The chosen geometry for the dot was the elliptical one, since this kind of geometry involves less loosing definition problems.

The samples were arranged in rows. In the case of 1 ink, a first row contained 7 samples corresponding to patches where the occupation area of C, M, Y and K was gradually increased from 20% to 80% in 10% steps. A second row contained 1 patch more, corresponding to the selected primary in full occupation ($a_1 = 100\%$).

Table 1. Angulations Employed for the Color Samples

HALFTONE	C	M	Y	K
1 ink	108.4	161.6	90.0	112.5
2 inks	135.0	15.0	75.0	-

In the case of 2 inks, the first row contained 7 patches again, but this time one of primaries was fixed at an occupation area of 20%, and the other was increased from 20% to 80% in 10% steps. In the second row, the primary that had previously varied was fixed, and the one that was previously fixed varied from 20% to 80% in 10% steps. A third row contained 3 patches more, corresponding to both inks at full occupation and the egalitarian mixture of them ($a_1 = 50\%$ and $a_2 = 50\%$). 2 more patches were also printed on the right-hand side of the surface for quality control purposes.

Each sample was named after the corresponding colors and occupation areas; e.g., Y30 refered to a sample of 1 ink where the occupation of the yellow was 30%, whereas C20M30 refered to a sample of 2 inks with a 20% of cyan and 30% of magenta. **Figure 1** shows an example of cyan and magenta. On the right hand side of the image a zoom of one of the patches has been included. It is important to remark that these percentages are the theoretical ones, that is to say, those imposed to the digital files. The real occupation would vary according to the accurateness of the printing system.

Altogether 67 halftones were created, 28 of 1 ink and 39 of 2 inks. **Table 1** shows the angulations of each primary in the case of 1 and 2 inks, where the angle origin is the negative horizontal axis (as considered by the software employed in the recreation of the halftones). For 1 ink, we assumed the typical angulation provided by the software, with the exception of the black, which was printed, like the 2 inks halftones, with the angle proposed by the bibliography.[11]

4.2 Transfer of the samples to the ceramic substrate

The different digital files were printed by means of an industrial CMYK Inkjet printer on 20×30 cm^2 engobed,

glazed and fired biscuit bases (for better consistency). After printing, the tiles underwent a 45 min firing cycle in a laboratory furnace. Therefore, the final ceramic parts were double-firing manufactured.

5. Measurement of the reflectance curves of the printed samples

For the obtaining of the experimental reflectance curves, as much as the reflectance of each primary at full occupation, we measured a 8 mm radius circle of each sample, with an integrating sphere MINOLTA CM-508i spectrophotometer, with illumination-geometry D65/10°. The spectral range covered was [400–700] nm (the one perceptible for the human eye), in 10 nm steps.[12] We take 5 readings of each sample, calculating the final reflectance as an average. The dispersion error associated to this measure, obtained by the formula:

$$\xi_d(R(\lambda_t)) = \sqrt{\frac{\Sigma_{j-1}^{5}(R_j(\lambda_t) - R_m(\lambda_i))^2}{5}}$$

was typically less than 2 orders of magnitude smaller in comparison with the average reflectance. Therefore this error would be included in the size of the represented dots and could be taken as acceptable.

6. Optimisation

Once the experimental reflectance values were measured, we had the necessary data to calculate the parameters of the 4 CPM. The obtaining of the parameters of a particular model which better fit to a set of experimental data could be estimated (from a mathematical point of view) employing optimisation techniques.[13)–16)] Next we present the global characteristics of this process in our study.

6.1 Optimization restrictions

Since the parameter ai relates to the percentage of occupied area of each primary color, 2 restrictions should be contemplated for any kind of optimization:

(1) The parameters must be equal or higher than 0, i.e. $a_i \geq 1,\ \forall i$

(2) The adding must be equal to 1, i.e. $\Sigma_i a_i = 1$

The inclusion of these restrictions in the optimization procedure allowed eliminating senseless solutions.

On the other hand, n relates to the light dispersion on the printed area, and so the fact of restricting its value to a "sensible" range is not easy. Nevertheless, it is know that in the case of surfaces where there is no light dispersion, n should take a value close to 1, whereas for perfect dispersion surfaces (Lambertian Surfaces), the value should be close to 2, although other researches justify the usage of values of n even of 10.[17)] In our study we have considered values between 20 and 30, in accordance to.[18)]

6.2 Optimization techniques

We used a Least Squares Adjustment for the linear models Marry–Davies and Neugebauer, with Linear Inequality Restrictions for Neugebauer. For the non-linear models Yule–Nielsen and Neugebauer Modified Yule–Nielsen we employed Preconditioned Combined Gradients, defining Confidence Regions for Yule–Nielsen, which where validated with the Neugebauer Modified Yule–Nielsen results.

The full development of the optimization process would divert this paper to the mathematical side of the research extensively, which is not part of the objective of this article. Therefore, we recommend consulting the bibliography for a detailed exposition.[13)–16)]

7. Definition of the merit figures

In order to compare experimental and analytic results, it was necessary to define some criteria, which could offer an objective (numeric) evaluation of the performance of the CPM. We assumed the following ones, considered in the bibliography.[19)]

(1) Root Mean Square Error (RMS): $RMS = ((\Sigma_\lambda (R(\lambda) - R_S(\lambda))^2)/N)^{0.5}$, where $N = 32$, i.e. the number of wavelengths in the interval [400, 700] nm, in 10 nm steps.

(2) CIE Delta $E_{L^*a^*b}$ color difference

(3) CIE Delta E_{00} color difference

(4) Metameric Index MI_{00}

In order to obtain the color difference by means of the formula CIEDE2000 it is necessary to begin from the coordinates of the color in the CIE–L*a*b color space.[20),21)] For the change $R(\lambda) \rightarrow (L^*a^*b)$ it is possible to start from the transformation of the reflectance curves to the (X, Y, Z) space employing the following equations:

$$X = K\sum_\lambda P(\lambda)R(\lambda)x(\lambda)$$

$$Y = K\sum_\lambda P(\lambda)R(\lambda)y(\lambda)$$

$$Z = K\sum_\lambda P(\lambda)R(\lambda)z(\lambda)$$

where $x(\lambda)$, $y(\lambda)$, $z(\lambda)$ are the Supplementary Standard Observatory Egalitarian Color Functions of 1964 (10°); P is the potency related to the D65 illuminate (the one used in the experiment), and K is a normalisation constant:

$$K = \frac{100}{\Sigma_\lambda P(\lambda)y(\lambda)}$$

so that for the Perfect Diffuser $(R(\lambda) = 1\ \forall\lambda)$ it is true that $Y = 100$. For the conversion of XYZ to L*a*b, we employed the conventional formulas, with [Xn, Yn, Zn] = [94.826, 100, 100.379]. The transformation Delta $E_{L^*a^*b} \rightarrow$ Delta E_{00} can be performed in 3 steps. For a more detailed explanation of this formula please see.[21)]

The obtaining of the Metameric Index MI_{00}[22)] between the two reflectance curves for a particular illuminate is based in the so called Parametric Decomposition,[23)] which allows to transform one reflectance spectrum in another so that the last one is a metamer of the referent, under a particular illuminate.

Additionally, it is convenient to mention that for the last years more criteria have been developed for the comparison of spectra, for instance.[24)–26)]

8. Results and discussion

The following tables show the results of the different optimizations on the different CPM. For the analysis of these results there is little bibliography where values of, for instance, the parameter RMS, are explicitly established for the evaluation of CPM. Nevertheless, in[27)] it is established that good results are those for which RMS < 1%. With regard to the Metameric Index, this should be less than 1 ($MI_{00} < 1$).

Table 2. Optimization Results for the Murray–Davies Model

SAMPLE	Area	Error RMS(%)	Delta ELAB	Delta E00	MI00
C20	0,29	0,60	0,83	1,20	0,01
C30	0,43	0,67	1,02	1,43	0,03
C40	0,55	0,71	1,09	1,49	0,03
C50	0,63	0,67	1,06	1,42	0,02
C60	0,73	0,56	0,89	1,15	0,02
C70	0,80	0,50	0,76	0,93	0,01
C80	0,87	0,40	0,57	0,65	0,02
M20	0,29	1,76	3,29	3,26	0,50
M30	0,42	1,98	4,07	3,44	0,47
M40	0,54	1,96	4,27	3,20	0,43
M50	0,64	1,88	4,34	2,96	0,40
M60	0,74	1,59	3,92	2,44	0,31
M70	0,82	1,31	3,41	1,96	0,27
M80	0,90	1,01	2,63	1,35	0,21
Y20	0,34	1,38	1,92	1,28	0,04
Y30	0,47	1,62	2,22	1,36	0,06
Y40	0,58	1,72	2,42	1,42	0,06
Y50	0,66	1,63	2,39	1,33	0,06
Y60	0,74	1,48	2,21	1,18	0,05
Y70	0,81	1,16	1,67	0,86	0,07
Y80	0,88	0,79	1,00	0,47	0,09
K20	0,32	1,84	2,63	2,82	0,13
K30	0,51	2,11	3,69	3,66	0,21
K40	0,67	1,99	4,33	3,92	0,21
K50	0,78	1,65	4,34	3,80	0,21
K60	0,87	1,19	3,75	3,20	0,17
K70	0,91	0,92	3,25	2,73	0,15
K80	0,95	0,55	2,18	1,81	0,10
Maximum.		2,11	4,34	3,92	0,21
Minimum.		0,40	0,57	0,47	0,01
Average		1,27	2,50	2,03	0,16

Table 3. Optimization Results for the Yule–Nielsen Model with $n=20$

SAMPLE	Area	Error RMS(%)	Delta ELAB	Delta E00	MI00
C20	0,24	0,30	0,46	0,67	0,03
C30	0,37	0,36	0,55	0,78	0,05
C40	0,48	0,41	0,60	0,82	0,05
C50	0,57	0,37	0,57	0,77	0,05
C60	0,67	0,30	0,44	0,58	0,03
C70	0,76	0,27	0,38	0,46	0,02
C80	0,84	0,21	0,31	0,31	0,00
M20	0,20	0,65	1,21	1,11	0,17
M30	0,31	0,73	1,35	1,04	0,10
M40	0,42	0,78	1,30	0,91	0,06
M50	0,52	0,70	1,28	0,84	0,07
M60	0,63	0,65	1,11	0,70	0,04
M70	0,73	0,42	0,98	0,57	0,06
M80	0,84	0,38	1,01	0,50	0,08
Y20	0,24	1,00	1,41	0,96	0,21
Y30	0,35	1,16	1,59	0,98	0,23
Y40	0,45	1,32	1,75	1,04	0,25
Y50	0,54	1,31	1,73	0,99	0,23
Y60	0,63	1,19	1,61	0,89	0,19
Y70	0,71	0,78	1,11	0,59	0,10
Y80	0,80	0,33	0,54	0,25	0,02
K20	0,17	1,14	1,60	1,81	0,05
K30	0,31	1,21	2,12	2,15	0,07
K40	0,45	1,11	2,46	2,18	0,07
K50	0,59	0,92	2,49	2,12	0,07
K60	0,72	0,67	2,18	1,80	0,06
K70	0,79	0,53	1,97	1,61	0,06
K80	0,88	0,33	1,36	1,10	0,04
Maximum.		1,32	2,49	2,18	0,25
Minimum.		0,21	0,31	0,25	0,02
Average		0,70	1,27	1,02	0,09

Table 4. Optimization Results for the Yule–Nielsen Model with $n=30$

SAMPLE	Area	Error RMS(%)	Delta ELAB	Delta E00	MI00
C20	0,24	0,30	0,45	0,66	0,03
C30	0,37	0,35	0,54	0,77	0,05
C40	0,48	0,40	0,59	0,81	0,05
C50	0,57	0,37	0,56	0,76	0,05
C60	0,67	0,30	0,44	0,57	0,03
C70	0,76	0,26	0,38	0,46	0,02
C80	0,84	0,21	0,30	0,31	0,00
M20	0,20	0,63	1,17	1,07	0,17
M30	0,31	0,71	1,30	1,00	0,09
M40	0,42	0,77	1,26	0,88	0,06
M50	0,52	0,69	1,23	0,81	0,06
M60	0,63	0,64	1,07	0,67	0,03
M70	0,73	0,41	0,94	0,55	0,05
M80	0,84	0,37	0,98	0,49	0,07
Y20	0,24	1,00	1,40	0,95	0,22
Y30	0,35	1,16	1,58	0,98	0,23
Y40	0,44	1,32	1,74	1,04	0,25
Y50	0,53	1,31	1,72	0,98	0,23
Y60	0,62	1,19	1,60	0,88	0,20
Y70	0,71	0,78	1,11	0,59	0,10
Y80	0,80	0,32	0,53	0,25	0,02
K20	0,17	1,13	1,58	1,79	0,05
K30	0,30	1,19	2,09	2,12	0,07
K40	0,45	1,10	2,42	2,15	0,07
K50	0,58	0,91	2,45	2,09	0,07
K60	0,71	0,66	2,15	1,77	0,06
K70	0,79	0,53	1,95	1,59	0,05
K80	0,88	0,32	1,35	1,09	0,04
Maximum.		1,32	2,45	2,15	0,25
Minimum.		0,21	0,30	0,31	0,00
Average		0,69	1,25	1,00	0,09

8.1 Murray–Davies and Yule–Nielsen models

Tables 2, **3** and **4** show, for the application of the Murray–Davies and Yule–Nielsen models on 1 ink samples, the results corresponding to the a_1 parameter (area), the RMS Error, the color differences Delta $E_{L^*a^*b}$ and Delta E_{00}, and Metameric Index MI_{00} of this late color difference, in the step of the illuminate D65 to A. It is also shown, apart from the 4 merit figures of each individual sample, the average, minimum and maximum of the total.

In the case of Yule–Nielsen, the optimization was performed for $n=20$ and $n=30$, in order to establish a good value of n for a ceramic substrate:

In order to evaluate the best value for the parameter n, the subsequent variations were calculated which are exposed in **Tables 5** and **6**:

From the two previous tables, we concluded that the increase in the quality of the Yule–Nielsen model prediction is small in the change from $n=20$ to $n=30$, in comparison with the quality increase in the change from the Murray–Davies to the Yule–Nielsen model for $n=20$. So that, we decide to take up $n=20$ for the optimization of the 2 inks models Neugebauer and Neugebauer Modified Yule–Nielsen.

8.2 Neugebauer and neugebauer modified Yule–Nielsen models

Tables 7 and **8** show, for the application of the Neugebauer and Neugebauer Modified Yule–Nielsen models on 2 inks samples, the results corresponding to the RMS Error, the color differences Delta $E_{L^*a^*b}$ and Delta E_{00}, and Metameric Index MI_{00} of this late color difference, in the step of the illuminate D65 to A. It is also exposed, apart from the 4 merit figures of each individual sample, the average, minimum and maximum of the total.

Table 5. Relative Variation between the Prediction of the Murray–Davies and Yule–Nielsen Models with $n = 20$

SAMPLE	Var.Error RMS(%)	Var.Delta ELAB(%)	Var.Delta E00(%)	Var. MI00(%)
C20	-49,79	-44,87	-44,08	82,14
C30	-46,89	-45,60	-45,20	81,75
C40	-42,55	-45,39	-44,98	78,82
C50	-44,33	-46,17	-45,65	82,66
C60	-46,76	-50,13	-49,57	110,60
C70	-46,50	-49,30	-50,23	60,61
C80	-46,49	-46,21	-51,27	-75,93
M20	-63,28	-63,36	-65,85	-65,63
M30	-63,32	-66,83	-69,61	-79,46
M40	-60,32	-69,52	-71,61	-85,76
M50	-62,76	-70,54	-71,67	-83,73
M60	-59,26	-71,64	-71,38	-88,16
M70	-68,13	-71,39	-70,91	-78,70
M80	-62,26	-61,57	-62,73	-63,65
Y20	-27,53	-26,18	-25,26	383,52
Y30	-28,28	-28,49	-27,81	311,03
Y40	-23,03	-27,80	-26,38	294,22
Y50	-20,10	-27,53	-25,70	281,65
Y60	-19,60	-27,43	-25,11	254,41
Y70	-32,84	-33,38	-30,69	43,62
Y80	-58,60	-46,41	-45,80	-83,97
K20	-38,02	-39,00	-35,96	-61,47
K30	-42,78	-42,52	-41,10	-66,78
K40	-44,11	-43,25	-44,42	-67,26
K50	-44,16	-42,71	-44,20	-66,83
K60	-43,77	-41,94	-43,81	-65,86
K70	-41,76	-39,29	-41,15	-63,78
K80	-40,29	-37,54	-39,10	-60,46
Average	-45,27	-46,64	-46,83	

Table 6. Relative Variation between the Prediction of the Murray–Davies and Yule–Nielsen Models with $n = 30$

SAMPLE	Var.Error RMS(%)	Var.Delta ELAB(%)	Var.Delta E00(%)	Var. MI00(%)
C20	-1,71	-1,47	-1,43	1,57
C30	-1,23	-1,45	-1,46	1,09
C40	-0,94	-1,42	-1,41	0,97
C50	-1,03	-1,44	-1,43	0,88
C60	-1,10	-1,69	-1,64	1,26
C70	-1,25	-1,66	-1,69	1,89
C80	-1,44	-1,44	-1,72	-5,13
M20	-3,30	-3,30	-3,48	-3,60
M30	-2,50	-3,58	-3,82	-7,15
M40	-1,43	-3,59	-3,67	-10,13
M50	-1,58	-3,76	-3,71	-9,23
M60	-0,87	-3,70	-3,44	-11,65
M70	-2,31	-4,01	-3,74	-6,57
M80	-2,68	-2,69	-2,75	-2,77
Y20	-0,04	-0,81	-0,81	1,49
Y30	-0,02	-0,79	-0,75	1,72
Y40	0,08	-0,66	-0,60	1,59
Y50	0,16	-0,55	-0,50	1,65
Y60	0,18	-0,44	-0,40	1,71
Y70	0,01	-0,49	-0,46	2,69
Y80	-1,01	-0,63	-0,59	5,96
K20	-1,37	-1,40	-1,20	-0,60
K30	-1,56	-1,53	-1,39	-3,23
K40	-1,50	-1,48	-1,49	-1,57
K50	-1,37	-1,34	-1,38	-1,87
K60	-1,22	-1,21	-1,27	-1,63
K70	-1,08	-1,03	-1,09	-2,16
K80	-0,95	-0,91	-0,96	-1,93
Average	-1,18	-1,73	-1,72	

Table 7. Optimization Results for the Neugebauer Model

SAMPLE	Error RMS(%)	Delta ELAB	Delta E00	MI00
C20M20	1,05	1,60	1,48	0,34
C20M30	1,29	2,05	1,76	0,43
C20M40	1,40	2,47	1,95	0,43
C20M50	1,44	2,77	2,02	0,38
C20M60	1,24	2,40	1,60	0,30
C20M70	1,08	2,54	1,56	0,24
C20M80	0,78	1,85	1,04	0,13
C30M20	1,01	1,53	1,35	0,37
C40M20	0,92	1,26	1,08	0,40
C50M20	1,13	2,04	1,57	0,29
C60M20	0,97	1,69	1,26	0,27
C70M20	0,95	1,88	1,33	0,15
C80M20	0,74	1,35	1,04	0,15
C20Y20	1,73	1,01	1,06	0,17
C20Y30	1,88	1,39	1,27	0,20
C20Y40	1,75	2,10	1,55	0,14
C20Y50	1,54	1,85	1,34	0,13
C20Y60	1,47	1,33	1,09	0,15
C20Y70	1,43	0,96	0,87	0,15
C20Y80	0,94	0,87	0,68	0,06
C30Y20	1,56	1,69	1,62	0,10
C40Y20	1,57	1,71	1,70	0,10
C50Y20	1,48	1,61	1,56	0,08
C60Y20	1,54	1,72	1,53	0,10
C70Y20	1,53	1,92	1,60	0,07
C80Y20	1,53	1,29	1,01	0,12
M20Y20	1,73	2,41	2,51	0,53
M20Y30	1,91	2,75	2,47	0,55
M20Y40	1,90	2,77	2,07	0,55
M20Y50	1,86	1,71	1,17	0,61
M20Y60	1,70	1,68	1,13	0,60
M20Y70	1,62	0,84	0,66	0,59
M20Y80	1,47	1,60	1,28	0,58
M30Y20	1,72	2,36	2,38	0,50
M40Y20	1,69	2,30	2,10	0,50
M50Y20	1,58	2,35	1,97	0,50
M60Y20	1,47	2,25	1,69	0,45
M70Y20	1,24	2,25	1,55	0,35
M80Y20	1,10	2,04	1,27	0,29
Maximum.	1,91	2,77	2,51	0,61
Minimum.	0,74	0,84	0,66	0,06
Average	1,41	1,85	1,49	0,31

As said, in the case of Neugebauer Modified Yule–Nielsen, the optimization was performed for $n = 20$:

9. Conclusions

According to the results offered by the tables exposed in the previous section, we concluded the following.

First, it is possible to evaluate the prediction quality of CPM on ceramic substrates, since the values obtained for the parameters $\{a_i, n\}$ are sensible in comparison with the theoretical ones and those obtained by other techniques, such as image segmentation.[28),29)]

Secondly, the non-linear models are more accurate than the linear ones. This is due to the existence of the n parameter, which models the optical dot gain. The inexistence of this factor in the linear models forces the a_i parameters to be systematically higher, so that they can reflect both, physical and optical dot gain. The introduction of a non-linear factor in a naturally non-linear process (light diffusion in a surface printed on a ceramic substrate) produces a remarkable improvement in the prediction quali-

Table 8. Optimization results for Neugebauer Modified Yule–Nielsen model with $n=20$

SAMPLE	Error RMS(%)	Delta ELAB	Delta E00	MI00
C20M20	0,63	0,43	0,39	0,19
C20M30	0,72	0,59	0,47	0,22
C20M40	0,69	0,68	0,50	0,21
C20M50	0,65	0,78	0,54	0,18
C20M60	0,52	0,53	0,34	0,13
C20M70	0,37	0,45	0,27	0,08
C20M80	0,29	0,39	0,21	0,03
C30M20	0,69	0,47	0,41	0,22
C40M20	0,70	0,47	0,39	0,25
C50M20	0,80	0,74	0,55	0,12
C60M20	0,78	0,65	0,46	0,08
C70M20	0,65	0,99	0,72	0,08
C80M20	0,49	0,78	0,50	0,04
C20Y20	0,60	0,90	0,70	0,01
C20Y30	0,69	1,05	0,75	0,03
C20Y40	0,67	1,02	0,70	0,03
C20Y50	0,60	0,94	0,63	0,03
C20Y60	0,55	0,93	0,60	0,03
C20Y70	0,46	0,77	0,50	0,02
C20Y80	0,47	0,60	0,37	0,01
C30Y20	0,61	0,79	0,71	0,01
C40Y20	0,62	0,79	0,75	0,01
C50Y20	0,60	0,79	0,73	0,01
C60Y20	0,59	0,82	0,72	0,01
C70Y20	0,59	0,88	0,76	0,01
C80Y20	0,59	0,93	0,80	0,02
M20Y20	0,87	1,29	1,06	0,05
M20Y30	1,04	1,51	1,06	0,05
M20Y40	1,09	1,58	0,99	0,05
M20Y50	0,93	1,54	0,89	0,09
M20Y60	0,77	1,43	0,79	0,14
M20Y70	0,62	0,61	0,32	0,18
M20Y80	0,73	0,49	0,40	0,28
M30Y20	1,02	1,27	1,02	0,04
M40Y20	1,08	1,32	1,00	0,04
M50Y20	0,91	1,28	0,94	0,05
M60Y20	0,68	1,11	0,78	0,06
M70Y20	0,54	0,98	0,67	0,04
M80Y20	0,36	0,79	0,51	0,07
Maximum.	1,09	1,58	1,06	0,25
Minimum.	0,29	0,39	0,21	0,01
Average	0,67	0,88	0,64	0,08

ty of the CPM, which is, in the end, quite logical. Then, the Yule–Nielsen model is more suitable than the Murray–Davies model for 1 ink halftones, and the Neugebauer Modified Yule–Nielsen model is more adequate than Neugebauer model for 2 inks halftones.

Finally, together with the research carried out by Iovine et al.[30] on a ceramic substrate, we can state that $n=20$ is an adequate value when employing the Yule–Nielsen and Neugebauer Modified Yule–Nielsen models on ceramic substrates.

Acknowledgements This work has been partially funded by the European Commission within the V Frame Programme, Project MONOTONE (G1RDCT–2002–00783).

References

1) B. Defez, "Analysis and definition of the optimal design of the back relieve in ceramic tile floorings by means of finite elements," Doctoral Thesis, Polytechnic University of Valencia (2007).
2) Ceramic Technology Institute of Castellon (Spain), "Action plan for the diminution of chromatic dispersion in the production of ceramic tiles by single-firing," Technical Report (1993).
3) G. Peris-Fajarnés, "Analysis of the serigraphic printing parameters that affect the chromatic variation found in ceramic tiles manufactured by single-firing," Doctoral Thesis, Polytechnic University of Valencia (1997).
4) I. Tortajada, G. Peris-Farjarnés, M. Aguilar and P. Latorre, *Bol. Soc. Esp. Ceram. Vidr.*, 45[1], 22–27 (2006).
5) R. Massen, *Ceram. Ind.*, 33, 38–41 (1999).
6) Working document of the V Frame Programme Project MONOTONE (2003), G1RD–CT–2002–00783 (2003).
7) A. Campbell, "The Designer's Lexicon," Chronicle Editorial, San Francisco (2000).
8) W. Hainke, "Serigraphy. Technique. Application. History," Ediciones La Isla (1979).
9) I. Tortajada, G. Peris-Fajarn'es and P. Latorre, "Informática y Artes Graficas," Polytechnic University of Valencia (2002).
10) D. Wyble and R. S. Berns, *Color Res. Appl.*, 25, 4–19 (2000).
11) J. Yule, "Principle of colour reproduction," John Wiley Sons, New York (1997).
12) Contact Spectrophotometer MINOLTA CM–508i," http://www.minoltaeurope.com (2004).
13) C. L. Lawson and R. J. Hanson, "Solving Least-squares Problems," SIAM Classics in Applied Mathematics (1995).
14) A. Sen and M. Srivastava, "Regression Analysis. Theory, Methods and Applications," Springer Text in Statistics, New York (1997).
15) L. E. Scales, "Introduction to Non-lineal Optimization," McMillan Computer Science Series (1985).
16) E. Castillo, A. Conejo, J. P. Pedregal, R. Garca and N. Alguacil, "Building and Solving Mathematical Programming Models in Engineering and Science," Pure and Applied Mathematics Series, Wiley-New York (2002).
17) R. Balasubramanian, *J. Electron. Imaging*, 8, 156–166 (1999).
18) P. Latorre, "Aplicación de modelos de predicción del color a impresiones de medios tonos sobre baldosa cerámica mediante impresora binaria de inyección de tinta (CMYK)". Doctoral Thesis, Polytechnic University of Valencia (2005).
19) L. Taplin and A. R. S. Berns, "Spectral color reproduction based on a six-color inkjet output system," Proc. of Ninth Color Imaging Conference: Color Science and Engineering, Systems, Technologies and Applications (IST), (2000) 209–213.
20) G. M. Johnson and M. D. Fairchild, *Color Res. Appl.*, 28, 425–435 (2003).
21) G. Sharma, W. Wu and E. N., Dalal, "The CIEDE2000 Colour Difference Formula: Implementation Notes, Supplementary Test Data, and Mathematical Observations," *Color Research*, 30 (2005).
22) L. Nimeroff and J. A. Yurow, *J. OPT. SOC. AM.*, 55, 185–190 (1965).
23) H. S. Fairman, "Metameric Correction using Parametric Decomposition," *Color Res. Appl.*, 12 261–265 (1987).
24) F. H. Imai, M. S. Rosen and R. S. Berns, "Comparison of spectrally narrow-band capture versus wide-band with a priori sample analysis for spectral reflectance estimation," Proc. Of the IST/SID Eighth Color Imaging Conference (2000) pp. 234–241.
25) J. A. Stephen-Viggiano,"Metrics for evaluating spectral matches: A quantitative comparison," Proc. of CGIV2004: The Second European Conference on Colour, Graphics, Imaging and Vision (2004).
26) D. Kalenova, P. Toivanen and V. Botchko, "Color Differences in a Spectral space," Proc. of CGIV2004: The Second European Conference on Colour, Graphics, Imaging

and Vision (2004).
27) F. H. Imai, D. R. Wyble and R. S. Bern, "A Feasibility Study of Spectral color Reproduction,"Imaging Sci. Techn., Vol. 47 (2003).
28) P. Latorre, G. Peris-Fajarnés, M. Mirmehdi and B. Thomas, "Assessing the Neugebauer Colour prediction model for ink-jet printed ceramic tiles". 4th. IASTED International Conference on Visualization, Imaging and Image Processing, Marbella (2004).
29) P. Latorre, "Aplicación de modelos de predicción del color a impresiones de medios tonos sobre baldosa cerámica mediante impresora binaria de inyección de tinta (CMYK)". Doctoral Thesis, Polytechnic University of Valencia (2005).
30) L. Iovine, S. Westland and T. L. V, Cheung, "Application of Neugebauer-based Models to Ceramic printing," IST/SID Twelfth Color Imaging Conference (2004) pp. 176–180.